

Spec SE mass spectrometer. Single-segment PSD spectra were recorded on isolated peptide $[M+H]^+$ ions. Phosphopeptides were sequenced (18) by nano-electrospray MS/MS on a Micromass Q-ToF. Precursor ion spectra for m/z 79 (14, 18) were recorded on a modified Sciex API III+ triple quadrupole mass spectrometer equipped with a nanospray source.

32. J. L. Joyal et al., *J. Biol. Chem.* **272**, 15419 (1997).
33. R. Verma et al., *Science* **278**, 455 (1997).

34. K. Biemann, *Methods Enzymol.* **193**, 886 (1990).

35. Immortalized *Xenopus* melanophores were cultured as described (36). For in vivo binding and release experiments, eight 100-mm plates of melanophores per treatment were each transfected by electroporation with 10 μ g of pcDNA3-myc-MGT or Ser¹⁶⁵⁰ mutants of this construct. Transiently transfected cells were allowed to express protein for 48 hours before harvest.

36. S. L. Rogers et al., *Proc. Natl. Acad. Sci. U.S.A.* **94**, 3720 (1997).

37. This work was supported by NIH grant GM-52111 and NSF grant MCB95-13388. We thank R. Larson and A. Murray for discussions; R. Deshaies for Plx1; and J. Hammer (NHLB, NIH) for pCMV2-FLAG-MC-ST.

27 March 2001; accepted 11 June 2001

Cohesin Cleavage by Separase Required for Anaphase and Cytokinesis in Human Cells

Silke Hauf, Irene C. Waizenegger, Jan-Michael Peters*

Cell division depends on the separation of sister chromatids in anaphase. In yeast, sister separation is initiated by cleavage of cohesin by the protease separase. In vertebrates, most cohesin is removed from chromosome arms by a cleavage-independent mechanism. Only residual amounts of cohesin are cleaved at the onset of anaphase, coinciding with its disappearance from centromeres. We have identified two separase cleavage sites in the human cohesin subunit SCC1 and have conditionally expressed noncleavable SCC1 mutants in human cells. Our results indicate that cohesin cleavage by separase is essential for sister chromatid separation and for the completion of cytokinesis.

In eukaryotes, replicated DNA molecules remain attached to each other until the onset of anaphase. This sister chromatid cohesion depends on a protein complex called cohesin (1). In yeast, sister chromatid separation is initiated by cleavage of cohesin's subunit Scc1p/Mcd1p by the protease separase (2, 3). This reaction removes cohesin from chromosomes and may directly dissolve cohesion between sister chromatids. In metaphase, separase is activated by the anaphase-promoting complex or cyclosome (APC), which mediates the ubiquitin-dependent proteolysis of the separase inhibitor securin (4–9).

In vertebrates, cohesin is removed from chromosomes in two steps. During prophase and prometaphase, the bulk of cohesin dissociates from the arms of condensing chromosomes (10) by a mechanism that depends neither on the APC-separase pathway nor on cleavage of the human ortholog of Scc1p/Mcd1p, SCC1 (11). A small amount of cohesin remains in centromeric regions until metaphase and is removed from chromosomes only at the onset of anaphase (9). In spread chromosomes from HeLa cells arrested in a preanaphase state, the absence of SCC1 staining on chromatid arms correlates

with the lack of arm cohesion (Fig. 1, A and B), supporting the notion that loss of cohesin is required for sister chromatid separation. The disappearance of residual amounts of SCC1 staining from centromeres coincides with the APC- and separase-dependent cleavage of a small amount of SCC1 (9). It is unknown, however, if this cleavage reaction, which affects maximally 10% of the total cellular cohesin, is required for anaphase.

To analyze the role of SCC1 cleavage in human cells, we identified two cleavage sites in SCC1. To map the NH₂-terminal site, we generated a series of in vitro-translated NH₂- and COOH-terminal truncation mutants of SCC1 and compared their electrophoretic mobilities to those of the COOH- and NH₂-terminal in vivo cleavage products, respectively (Fig. 1C). These analyses suggested that amino acid residues 168 to 182 contain the NH₂-terminal cleavage site. Comparison of this region with the recognition site consensus of yeast separase (2, 12, 13) suggested that human SCC1 is cleaved after Arg¹⁷² (Fig. 1D). The analysis of recombinant versions of SCC1 containing small deletions or point mutations in this region confirmed this hypothesis (Fig. 1E). The same strategy was used to identify Arg⁴⁵⁰ as the COOH-terminal SCC1 cleavage site (Fig. 1, D and E) (14). Mutation of both sites abolished SCC1 cleavage by separase in vitro (Fig. 1F). Comparison of these sites with known separase cleavage sites in budding and fission yeast (2,

12, 13) yields glutamate-X-X-arginine as the consensus for the sequence preceding the scissile peptide bond (Fig. 1D). In yeast, Cdc5p kinase mediates phosphorylation of serine residues at the P6 positions preceding the cleavage sites in Scc1p/Mcd1p, which enhances cleavage (15). In the NH₂-terminal cleavage site of human SCC1, this position is occupied by an aspartate residue, suggesting that separase prefers acidic residues at the P6 position.

We generated stable human HeLa cell lines in which physiologic amounts of wild-type or cleavage-site mutants of myc-tagged SCC1 are expressed upon addition of doxycycline (Fig. 2A) (16). Cell lines expressing noncleavable SCC1 proliferated more slowly than did lines expressing the wild-type or single-site mutants (14). Transgene expression was rapidly lost after expression of noncleavable SCC1 (Fig. 2B), indicating that the modified SCC1 interferes with proliferation. All SCC1 mutants were incorporated into 14S cohesin complexes (Fig. 2C) (14) and showed nuclear localization in interphase (Fig. 3H), implying that they acted as functional cohesin subunits. Fluorescence microscopy of mitotic cells (Fig. 2D) and incubation of chromatin fractions in meiotic *Xenopus* egg extracts (Fig. 2E) in which the APC-separase pathway is inactive (11, 17) suggested that the bulk of all SCC1 mutants can be dissociated from chromosomes by the prophase pathway, further demonstrating that this pathway does not depend on SCC1 cleavage. Analysis of SCC1 cleavage in mitotic *Xenopus* extracts using chromatin from the different HeLa cell lines as substrate confirmed that the different SCC1 mutants are noncleavable at either the NH₂- or the COOH-terminal site or at both (Fig. 2F).

Immunofluorescence microscopy suggested that most cells expressing wild-type SCC1 completed mitosis and cytokinesis normally (Fig. 3A), whereas multiple mitotic abnormalities were seen in cells expressing noncleavable SCC1 (Fig. 3B). In the latter cells, the cleavage furrow had often begun to ingress although anaphase had not occurred; i.e., the chromosomes remained at the spindle equator. In these cases, the cleavage furrow appeared to constrict the chromosome mass randomly in either a symmetric or an asymmetric manner (Fig. 3B), resembling the cut phenotype in fission yeast mutants defective in anaphase (18). No cyclin B staining could be observed in the human cells attempting

Research Institute of Molecular Pathology (IMP), Dr.-Bohr Gasse 7, A-1030 Vienna, Austria.

*To whom correspondence should be addressed. E-mail: peters@nt.imp.univie.ac.at

REPORTS

Fig. 1. (A and B) Localization of SCC1-myc on chromosomes of nocodazole-arrested cells. HeLa SCC1-myc cells were spread onto slides, extracted prior to fixation, and stained with antibody to myc (anti-myc; red), CREST serum (green), and 4',6'-diamidino-2-phenylindole (DAPI; blue) (16). **(C)** Mapping of SCC1 cleavage sites. In vitro transcribed and translated NH₂- or COOH-terminally truncated versions of human SCC1 were analyzed side by side with SCC1 cleaved in vivo (anaphase xt) by immunoblotting (16). Arrows indicate the in vivo cleavage products. The arrowhead marks full-length SCC1. Faster migrating bands in the right panel might result from internal translational starts or precocious translational stops. **(D)** Comparison of the two cleavage recognition sites of human SCC1 with putative (Mm, Xl, Dm) and with published (Sc, Sp) cleavage recognition sites in other species, leading to a minimal consensus sequence. An arrow indicates the peptide bond cleaved by separase (25). **(E)** SCC1 mutants with either point mutations or small deletions were in vitro transcribed and translated, and analyzed for their cleavability by incubation with activated separase as in (F) (16). **(F)** Activated separase was incubated with in vitro transcribed and translated wild-type SCC1-myc or with the NC mutant (input). At indicated time points, samples were taken and analyzed by immunoblotting with anti-myc. Arrows indicate both cleavage products of wild-type SCC1-myc.

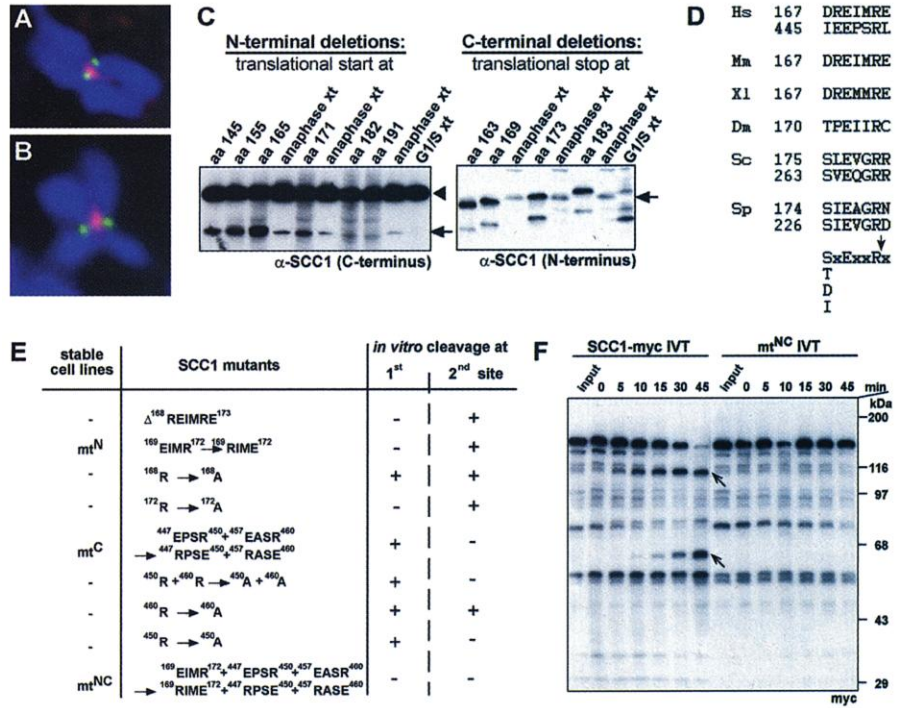
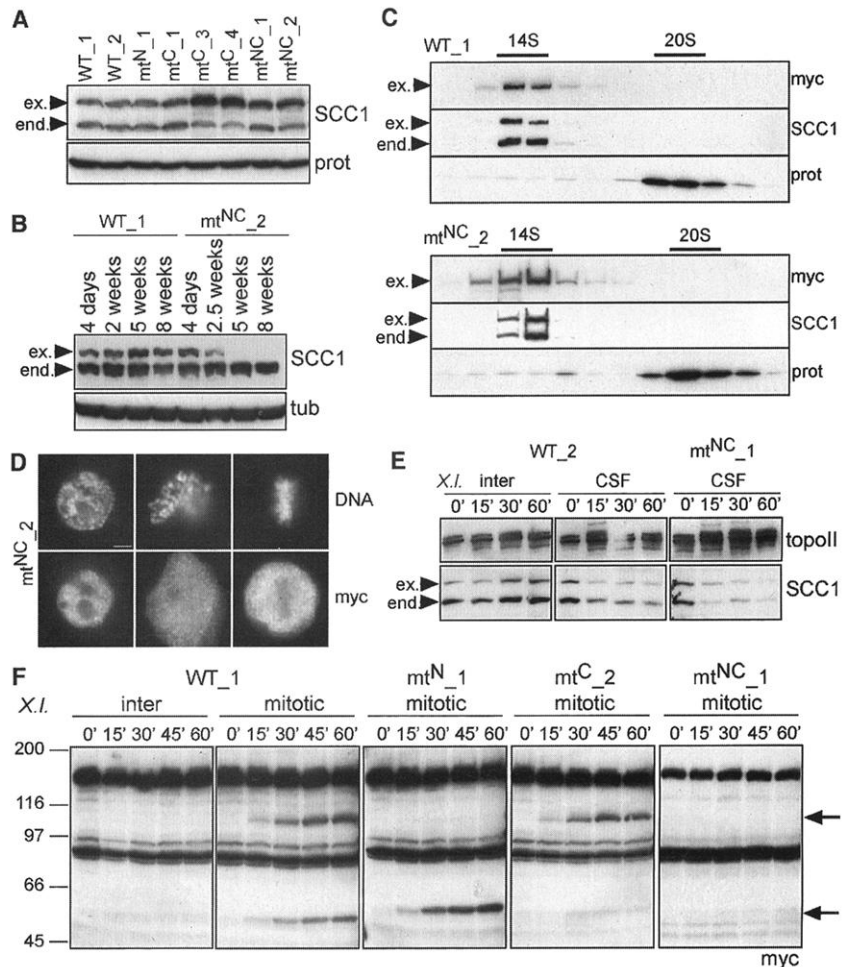


Fig. 2. Characterization of HeLa cell lines inducibly expressing the wild-type (WT) or mutant forms (mt^N, mt^C, mt^{NC}; Fig. 1E) of SCC1-myc. (A) Expression levels after 3 days of induction. SCC1 immunoblot of whole-cell extracts (9). Cell lines are indicated on top; numbers specify different clones expressing the same construct. Tagged exogenous SCC1 (ex.) can be separated from endogenous SCC1 (end.) because of its higher molecular mass. Loading control: anti-proteasome immunoblot (prot) (9). **(B)** Expression levels after different times of induction. Western blot of whole-cell extracts prepared at the indicated time points after induction. Loading control: anti- α -tubulin immunoblot (tub) (9). **(C)** Sucrose density gradient centrifugation of cell extracts (16). Exogenous SCC1 sediments with 14S indicating that it is incorporated into 14S cohesin complexes. **(D)** Fluorescence microscopy of cell line mt^{NC}₂ (16). Cells were stained with anti-myc, DNA was counterstained with DAPI. Cells in prophase, prometaphase, and metaphase are shown. Bar, 5 μ m. **(E)** In vitro dissociation assay. Crude chromatin pellets from logarithmically growing HeLa cell lines were incubated in interphase (inter) or CSF *Xenopus* egg extract (17) for the indicated periods of time. DNA was reisolated through a sucrose cushion and immunoblotted for topoisomerase II (topoII) and SCC1. **(F)** In vitro cleavage assay. Crude chromatin pellets from nocodazole-arrested HeLa cell lines were incubated in interphase (inter) or mitotic *Xenopus* egg extract (X.I.) (9). Samples were taken at the indicated time points and analyzed by immunoblotting with anti-myc. Arrows mark mitosis-specific SCC1 cleavage products.



cytokinesis in the absence of anaphase (14), implying that the APC and therefore presumably also separase had been activated. The Aurora-B kinase relocates from centromeres to the spindle midzone around the same time as SCC1 is cleaved (Fig. 3C) (19). Aurora-B could also be detected at the spindle midzone in cells that failed to separate their chromatids due to uncleavable SCC1 (Fig. 3, D and E), suggesting that Aurora-B relocation does not depend on chromatid separation. In addition, anaphase bridges were frequently observed in cells expressing noncleavable SCC1, but a significant fraction of cells also appeared to undergo anaphase normally (Fig. 3F). It is possible that cells undergoing a normal anaphase expressed less noncleavable SCC1 than did cells showing anaphase defects. Inspection of cells expressing SCC1 mutants that can only be cleaved at either one of the two cleavage sites revealed an increase in the frequency of cells with anaphase bridges, but no cells with the cut phenotype could be observed (Fig. 3F).

In interphase cells expressing noncleavable

SCC1, micronuclei, enlarged nuclei, and multiple nuclei were frequently observed (Fig. 3G). Fluorescence-activated cell sorting (FACS) (16) revealed that expression of noncleavable SCC1 coincided with a pronounced increase in aneuploid cells, representing, in some samples, 30% of all transgene-expressing cells (Fig. 3H). To analyze how cells with these phenotypes arise, we analyzed cells expressing SCC1 mutants and a green fluorescent protein (GFP)-tagged version of histone H2B (20) by video microscopy (16). Expression of wild-type SCC1 did not interfere with mitotic progression, whereas cells expressing noncleavable SCC1 initiated cytokinesis without segregating chromosomes (Fig. 4, A and B) (16). The latter cells stretched chromosomes toward the opposite poles of the cleaving cell and partially constricted the chromosomes by the ingressing cleavage furrow, causing the cut phenotype seen in fixed cells (Fig. 3B). Eventually, the cleavage furrow regressed, and the cells entered interphase without completing cytokinesis, often containing an enlarged and irregularly shaped nucleus (Fig. 4B).

To examine the karyotype of these cells, we

induced expression of noncleavable SCC1 for 3 days to allow on average one round of mitosis in the presence of noncleavable cohesin, then added colchicine to accumulate cells in the subsequent mitosis and analyzed chromosome spreads by microscopy (16). Many spreads contained diplochromosomes in which two pairs of sister chromatids were aligned in parallel, reminiscent of the chromosomes observed in *Drosophila* mutants defective in anaphase (21). Such karyotypes were infrequent in spreads from cells expressing wild-type SCC1 or single-site cleavage SCC1 mutants (Fig. 4C) (14). These observations suggest that cells expressing noncleavable SCC1 reenter interphase with sis-

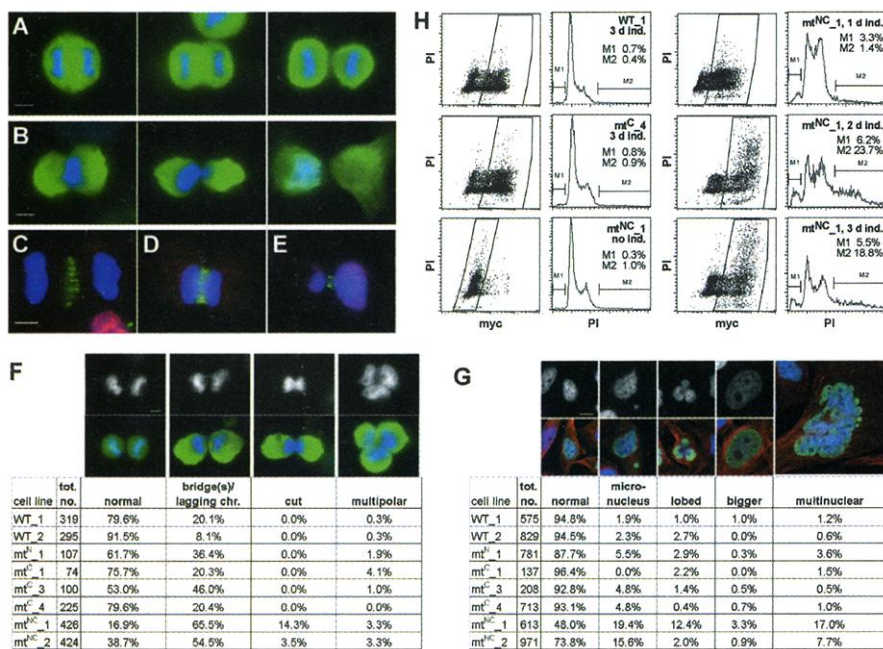


Fig. 3. Phenotype of HeLa cells expressing noncleavable SCC1-myc. (A) Normal mitoses in cells that expressed SCC1-myc WT (two left panels) or SCC1-myc mt^{NC} (right panel). Cells were stained with anti-myc (green) and DAPI (blue) (16). Bar, 5 μm. (B) Abnormal mitoses in cells that expressed hSCC1-myc mt^{NC}. Same staining as in (A). Bar, 5 μm. (C through E) Cells expressing hSCC1-myc WT (C) or hSCC1-myc mt^{NC} (D and E) were extracted prior to fixation and costained for Aurora-B (green) and hSCC1-myc (red). DNA was stained with DAPI (blue). Bar, 5 μm. (F) Morphology of cells undergoing cytokinesis determined 3 days after induction. Cells undergoing cytokinesis and expressing wild-type or mutant versions of SCC1-myc were classified as follows: (normal) normal anaphase or telophase, [bridge(s)/lagging chr.] cells in anaphase or telophase that showed either chromatid bridges or lagging chromosomes, (cut) cells undergoing cytokinesis without having separated their chromatid, (multipolar) multipolar anaphases or telophases. The total number (tot. no.) of cells counted for each cell line is indicated. Upper panel: DNA stained with DAPI. Lower panel: DNA in blue, SCC1-myc in green. Bar, 5 μm. (G) Morphology of interphase nuclei determined 5 to 7 days after induction. The total number (tot. no.) of cells counted for each cell line is indicated. Upper panel: DNA stained with DAPI. Lower panel: DNA in blue, α-tubulin in red, and SCC1-myc in green. Bar, 10 μm. (H) FACS analysis of DNA content. Cells were stained for SCC1-myc (myc) and DNA (propidium iodide, PI). Only cells gated for in the dot plot are shown in the histogram panel. The percentage of hypodiploid (M1) or hyperdiploid (M2) cells is indicated.

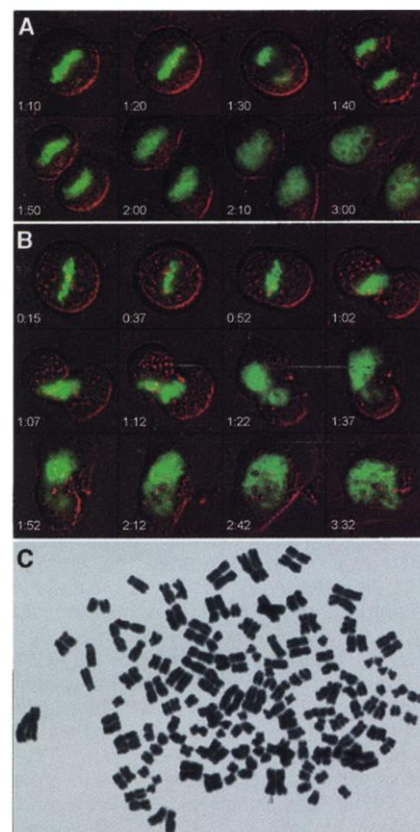


Fig. 4. Cells exhibiting a “cut” phenotype eventually fail to undergo cytokinesis, and diplochromosomes are present after 3 days of induction. Video microscopy of cells expressing wild-type (A) or noncleavable (B) SCC1-myc (16). Cell lines WT_1 and mt^{NC}_1 were stably transfected with H2B-GFP (20) to visualize DNA. Cells were induced to express SCC1-myc for 2 days before analysis. Selected pictures taken at the indicated time points (hours:min) are shown (representative of three recordings). Nomarski is shown in red, overlaid by H2B-GFP in green. (C) Chromosome spread of cells expressing noncleavable SCC1-myc. Cell line mt^{NC}_1 was induced to express SCC1-myc for 3 days. Mitotic cells were harvested after 2 hours treatment with colchicine, incubated in hypotonic solution, fixed, and spread. Coverslips were stained with Giemsa. Of the spreads in this preparation, 5.4% showed several diplochromosomes (compared to none in cell line WT_2).

ter chromatids still connected. These cells nevertheless re-replicate their DNA, resulting in the formation of diplochromosomes in the subsequent mitosis (Fig. 4C). Repeated cycles of abortive mitosis and DNA re-replication may cause formation of the polyploid or multinucleate cells observed by FACS and microscopy (Fig. 3). Paradoxically, spread diplochromosomes typically appeared as pairs of chromosomes whose centromeric regions were not connected (Fig. 4C). Their nonrandom parallel orientation on the coverslips can only be explained, however, by assuming that all four chromatids had been connected by cohesion prior to the hypotonic spreading procedure.

Our results suggest that cohesin cleavage is essential for sister chromatid separation and cytokinesis, even though only a minor amount of SCC1 is cleaved in mitosis (9). It is therefore likely that the anaphase defects of cells in which separase activity is compromised by securin overexpression or deletion are similarly caused by defects in SCC1 cleavage (22, 23). Because SCC1 cleavage coincides with the disappearance of cohesin from centromeres (9), SCC1 cleavage may preferentially dissolve cohesion at centromeres. It is possible that the cytokinesis defects induced by noncleavable cohesin are caused by a mechanical inability of the cleavage furrow to cut through chromosomes remaining in the furrow plane. Alternatively, it is conceivable that a surveillance mechanism prevents cytokinesis in the presence of unseparated sister chromatids.

Our observations also support the notion that sister separation is essential neither for cyclin B destruction and exit from mitosis nor for DNA re-replication in the next cell cycle (2, 4–8, 21) — and is also not necessary for relocalization of Aurora-B from centromeres to the spindle midzone. Naturally occurring defects in separase activation and SCC1 cleavage would therefore not simply block cell cycle progression, but could instead cause chromosome non-disjunction events that could subsequently cause continued chromosomal instability by initiating chromosome breakage-fusion-bridge cycles (24). It will therefore be of interest to determine if defects in separase regulation contribute to the genomic instability observed in human tumors.

References and Notes

1. K. Nasmyth, J. M. Peters, F. Uhlmann, *Science* **288**, 1379 (2000).
2. F. Uhlmann, F. Lottspeich, K. Nasmyth, *Nature* **400**, 37 (1999).
3. F. Uhlmann, D. Wernic, M. A. Poupart, E. V. Koonin, K. Nasmyth, *Cell* **103**, 375 (2000).
4. O. Cohen-Fix, J. M. Peters, M. W. Kirschner, D. Koshland, *Genes Dev.* **10**, 3081 (1996).
5. H. Funabiki *et al.*, *Nature* **381**, 438 (1996).
6. R. Ciosk *et al.*, *Cell* **93**, 1067 (1998).
7. H. Zou, T. J. McGarry, T. Bernal, M. W. Kirschner, *Science* **285**, 418 (1999).
8. O. Leisemann, A. Herzig, S. Heidmann, C. F. Lehner, *Genes Dev.* **14**, 2192 (2000).
9. I. C. Waizenegger, S. Hauf, A. Meinke, J. M. Peters, *Cell* **103**, 399 (2000).

10. A. Losada, M. Hirano, T. Hirano, *Genes Dev.* **12**, 1986 (1998).
11. I. Sumara, E. Vorlaufer, C. Gieffers, B. H. Peters, J. M. Peters, *J. Cell Biol.* **151**, 749 (2000).
12. S. B. Buonomo *et al.*, *Cell* **103**, 387 (2000).
13. T. Tomonaga *et al.*, *Genes Dev.* **14**, 2757 (2000).
14. S. Hauf, I. C. Waizenegger, J.-M. Peters, data not shown.
15. G. Alexandru, F. Uhlmann, K. Mechtler, M. Poupart, K. Nasmyth, *Cell* **105**, 459 (2001).
16. Supplementary material is available at Science Online at www.sciencemag.org/cgi/content/full/293/5533/1320/DC1.
17. E. Vorlaufer, J. M. Peters, *Mol. Biol. Cell* **9**, 1817 (1998).
18. M. Yanagida, *Trends Cell Biol.* **8**, 144 (1998).
19. E. A. Nigg, *Nature Rev. Mol. Cell Biol.* **2**, 21 (2001).
20. T. Kanda, K. F. Sullivan, G. M. Wahl, *Curr. Biol.* **8**, 377 (1998).
21. R. Stratmann, C. F. Lehner, *Cell* **84**, 25 (1996).
22. A. Zur, M. Brandeis, *EMBO J.* **20**, 792 (2001).
23. P. V. Jallepalli *et al.*, *Cell* **105**, 445 (2001).
24. B. McClintock, *Cold Spring Harbor Symp. Quant. Biol.* **9**, 72 (1941).
25. Single-letter abbreviations for the amino acid residues are as follows: A, Ala; C, Cys; D, Asp; E, Glu; F, Phe; G, Gly; H, His; I, Ile; K, Lys; L, Leu; M, Met; N, Asn; P, Pro; Q, Gln; R, Arg; S, Ser; T, Thr; V, Val; W, Trp; and Y, Tyr. X indicates any residue.
26. We thank K. Paiha and P. Steinlein for help with microscopy and FACS, A. H. F. M. Peters for advice on chromosome spreading, A. Kromminga for CREST serum, N. Redemann for Polo-like kinase, and T. Kanda and G. Wahl for the H2B-GFP construct. We are grateful to K. Nasmyth and members of the Peters lab for critically reading the manuscript. Supported by Boehringer Ingelheim and by a grant from the Austrian Science Fund (FWF P13865-BIO). S.H. was supported by a post-doctoral fellowship from the Deutscher Akademischer Auslandsdienst (DAAD).

5 April 2001; accepted 26 June 2001

Vascular Abnormalities and Deregulation of VEGF in *Lkb1*-Deficient Mice

Antti Ylikorkala,^{1*} Derrick J. Rossi,^{1*} Nina Korsisaari,¹ Keijo Luukko,² Kari Alitalo,^{1,3} Mark Henkemeyer,⁴ Tomi P. Mäkelä^{1,3,†}

The *LKB1* tumor suppressor gene, mutated in Peutz-Jeghers syndrome, encodes a serine/threonine kinase of unknown function. Here we show that mice with a targeted disruption of *Lkb1* die at midgestation, with the embryos showing neural tube defects, mesenchymal cell death, and vascular abnormalities. Extraembryonic development was also severely affected; the mutant placentas exhibited defective labyrinth layer development and the fetal vessels failed to invade the placenta. These phenotypes were associated with tissue-specific deregulation of vascular endothelial growth factor (VEGF) expression, including a marked increase in the amount of VEGF messenger RNA. Moreover, VEGF production in cultured *Lkb1*^{-/-} fibroblasts was elevated in both normoxic and hypoxic conditions. These findings place *Lkb1* in the VEGF signaling pathway and suggest that the vascular defects accompanying *Lkb1* loss are mediated at least in part by VEGF.

Germ line mutations of the *LKB1* gene cause Peutz-Jeghers syndrome, which is characterized by gastrointestinal polyposis, abnormal melanin pigmentation, and increased risk of cancer (1). The *Lkb1* gene encodes a serine/threonine kinase of unknown function with no identified in vivo substrates and a ubiquitous expression pattern during mouse development (2). To study the function of *Lkb1*,

we generated *Lkb1*-deficient mice.

Two independent gene-targeting strategies were used to functionally disrupt *Lkb1* in the murine germ line (3, 4). In *Lkb1* heterozygous (*Lkb1*^{+/-}) intercrosses, both *Lkb1*^{+/+} (n = 87) and *Lkb1*^{+/-} (n = 177) animals were observed at expected frequencies, whereas no *Lkb1*^{-/-} animals were obtained. Analysis of *Lkb1*^{-/-} embryos throughout embryonic development revealed no abnormalities before embryonic day 7.5 (E7.5), and most embryos appeared to develop normally up to E8.0. Macroscopic analysis of *Lkb1*^{-/-} embryos beyond E8.25 revealed multiple abnormalities, including a failure of the embryo to turn, a defect in neural tube closure, and a hypoplastic or absent first branchial arch (Fig. 1A). No viable embryos were recovered after E11.0, indicating that *Lkb1* is essential for embryonic development.

Whole-mount in situ hybridization was used to study the integrity of various developmental

¹Molecular and Cancer Biology Program, Haartman Institute and Biomedicum Helsinki, Post Office Box 63, University of Helsinki, Helsinki 00014, Finland. ²Department of Anatomy and Cell Biology, University of Bergen N-5009 Bergen, Norway. ³Helsinki University Central Hospital Laboratory Diagnostics, Post Office Box 401, Helsinki 00029 HYKS, Finland. ⁴Center for Developmental Biology, University of Texas Southwestern Medical Center, Dallas, TX 75235–9133, USA.

*These authors contributed equally to this work.

†To whom correspondence should be addressed. E-mail: tomi.makela@helsinki.fi